NEOPLASIA
www.neoplasia.com

Volume 18 Number 6 June 2016 pp. 387–397 387

Early Detection of Treatment-Induced Mitotic Arrest Using Temporal Diffusion Magnetic Resonance Spectroscopy[1,2]

Xiaoyu Jiang[*,†,‡], Hua Li[*,†,‡], Ping Zhao[*,†,‡], Jingping Xie[*,†,‡], Dineo Khabele[§,¶,#], Junzhong Xu[*,†,‡,#,,††,‡‡] and John C. Gore[*,†,‡,#,**,††,‡‡,§§,¶¶]**

*Institute of Imaging Science, Vanderbilt University, Nashville, TN 37232, USA; †Department of Radiology, Vanderbilt University, Nashville, TN 37232, USA; ‡Department of Radiological Sciences, Vanderbilt University, Nashville, TN 37232, USA; §Department of Obstetrics, Vanderbilt University, Nashville, TN 37232, USA; ¶Department of Gynecology, Vanderbilt University, Nashville, TN 37232, USA; #Vanderbilt-Ingram Cancer Center, Vanderbilt University, Nashville, TN 37232, USA; **Department of Physics, Vanderbilt University, Nashville, TN 37232, USA; ††Department of Astronomy, Vanderbilt University, Nashville, TN 37232, USA; ‡‡Department of Biomedical Engineering, Vanderbilt University, Nashville, TN 37232, USA; §§Department of Molecular Physiology, Vanderbilt University, Nashville, TN 37232, USA; ¶¶Department of Biophysics, Vanderbilt University, Nashville, TN 37232, USA

Abstract

PURPOSE: A novel quantitative magnetic resonance imaging (MRI) method, namely, temporal diffusion spectroscopy (TDS), was used to detect the response of tumor cells (notably, mitotic arrest) to a specific antimitotic treatment (Nab-paclitaxel) in culture and human ovarian xenografts and evaluated as an early imaging biomarker of tumor responsiveness. *METHODS:* TDS measures a series of apparent diffusion coefficients (ADCs) of tissue water over a range of effective diffusion times, which may correspond to diffusion distances ranging from subcellular to cellular levels (~3-20 μm). By fitting the measured ADC data to a tissue model, parameters reflecting structural properties such as restriction size in solid tumors can be extracted. Two types of human ovarian cell lines (OVCAR-8 as a responder to Nab-paclitaxel and NCI/ADR-RES as a resistant type) were treated with either vehicle (PBS) or Nab-paclitaxel, and treatment responses of both *in vitro* and *in vivo* cases were investigated using TDS. *RESULTS:* Acute cell size increases induced by Nab-paclitaxel in responding tumors were confirmed by flow cytometry and light microscopy in cell culture. Nab-paclitaxel–induced mitotic arrest in treated tumors/cells was quantified histologically by measuring the mitotic index *in vivo* using a mitosis-specific marker (anti-phosphohistone H3). Changes in the fitted restriction size, one of the parameters obtained from TDS, were able to detect and quantify increases in tumor cell sizes. All the MR results had a high degree of consistency with other flow, microscopy, and histological data. Moreover, with an appropriate analysis, the Nab-paclitaxel–responsive tumors *in vivo* could be easily distinguished from all the other vehicle-treated and Nab-paclitaxel–resistant tumors. *CONCLUSION:* TDS detects increases in cell sizes associated with antimitotic-therapy–induced

Address all correspondence to: John C. Gore, Vanderbilt University, Institute of Imaging Science, Nashville, TN 37232, United States.
E-mail: john.gore@vanderbilt.edu

[1] This study has been supported by National Institutes of Health grants R01CA109106 (to J. C. Gore) and R01CA173593 (to J. C. Gore).
[2] Disclosure of Potential Conflicts of Interest: No potential conflicts of interest were disclosed.

Received 4 February 2016; Revised 1 April 2016; Accepted 14 April 2016

1476-5586
http://dx.doi.org/10.1016/j.neo.2016.04.006

mitotic arrest in solid tumors *in vivo* which occur before changes in tissue cellularity or conventional diffusion MRI metrics. By quantifying changes in cell size, TDS has the potential to improve the specificity of MRI methods in the evaluation of therapeutic response and enable a mechanistic understanding of therapy-induced changes in tumors.

Neoplasia (2016) 18, 387–397

Introduction

Tumor progression relies upon abnormally frequent cell division. Microtubules play an important role in the process of cell division, so targeting microtubules with appropriate anticancer drugs continues to be a successful approach for cancer chemotherapy [1]. Several new drugs that target microtubules are being developed or are already in clinical trials. Among current microtubule-targeted agents, Nab-paclitaxel (Abraxane) is widely used to treat breast, ovarian, lung, and pancreatic cancers and Kaposi's sarcoma [2,3]. Despite the clinical success of this class of pharmaceuticals, drug resistance is a common occurrence [1]. Therefore, it is highly desirable to detect the early response of individual patients' tumors to successful, or unsuccessful, antimitotic therapies so that treatment regimens can be altered adaptively in time to minimize unnecessary toxicity and treatment delays. Measuring changes in tumor size by x-ray computed tomography or magnetic resonance imaging (MRI) [4], the current standard method to assess the treatment response of solid tumors, suffers from fundamental limitations [5,6]. Fine-needle aspiration has been used to detect paclitaxel-induced mitotic arrest in breast cancer. However, this approach has limitations which include the invasive nature of the procedure, applicability, and insufficient tissue collection [7]. Sequential positron emission tomography imaging using F-18-fluorodeoxyglucose has been reported to assess metabolic changes in ovarian cancer in a small group of patients receiving paclitaxel treatments, but the sensitivity and specificity of this method need further investigation [8].

Diffusion-weighted MRI (DW-MRI) is a noninvasive imaging technique that has previously been used to assess tumor treatment response without the need for any hazardous radiation or exogenous probes. DW-MRI reveals information on the random (Brownian) motion of water molecules in tissues. Water movement in tissues is modified by interactions with, e.g., hydrophobic cellular membranes, intracellular organelles, and macromolecules, so the observed rate of water diffusion in cellular tissues is less than that in free solutions. The apparent diffusion coefficient (ADC) that is measured by practical MRI methods thereby provides information on those factors that hinder or restrict free diffusion including tissue cell density and cell sizes, extracellular-space tortuosity, and the integrity of cellular membranes [9]. Preclinical and clinical data have indicated the potential role of DW-MRI in the monitoring tumor response to therapy [10–12]. It has been reported that ADC values for human breast cancer tumor xenografts increase in response to paclitaxel treatment and occur earlier than significant tumor volume reductions [13]. However, ADC values are potentially affected by multiple factors including tissue cellularity, cell size, nuclear size, cell membrane integrity, and the presence of necrosis [14,15], which are all commonly involved in the tumor response to therapies. Interpretation of these changing ADC values must, therefore, be made with caution [14,16].

The dynamics of the response to antimitotic drug have been investigated by time-lapse microscopy in culture [17]. As illustrated in Supplementary Figure 1, the treated tumor cells first enter mitotic arrest and then either initiate apoptosis or exit into an abnormal G_1-like state with multiple small nuclei. Most multinucleated cells cannot recover normal nuclear morphology and eventually die. Mitotic arrest has therefore long been established as a hallmark of the cellular response to antimitotic drugs. It has been widely used as a biomarker in human and rodent cancer models by scoring histology sections or stained biopsies [18,19]. A noninvasive imaging readout of this biomarker would allow a specific and accurate quantification of tumor response to antimitotic therapies which potentially occurs earlier than measureable tumor regression.

Temporal diffusion spectroscopy (TDS) is a specific class of DW-MRI which can characterize tissue microstructure more comprehensively than conventional single-ADC measurement and which may allow a more mechanistic understanding of chemotherapy-induced cellular changes [20–24]. Rather than measuring a single average ADC over a relatively long diffusion time (~20-50 milliseconds), TDS measures ADC values over a range of effective diffusion times, corresponding to diffusion distances ranging from subcellular to cellular levels (~3-20 μm). These are achieved by using time-varying (typically cosinusoidally oscillating) diffusion-sensitizing gradients in which the effective diffusion time is determined by the characteristic frequency of the gradient waveforms, and hence measured ADC values are expressed as a function of a spectral frequency. By fitting the measured ADC spectra to a simplified tissue model, three parameters associated with mean cell size, the tortuosity of the extracellular space, and a measure of intracellular structural complexity, respectively, can be extracted. It may be noted that both mitotic arrest and multinucleation act to increase mean tumor cell size [25]. The derived spectral parameter associated with cell size is hypothesized to reflect these dimensional increases and accordingly may provide a specific and accurate quantification of cellular response to antimitotic therapy. In the current study, this hypothesis is evaluated in cell cultures *in vitro* and in human ovarian cancer xenografts *in vivo*. The MR results are supported by flow cytometry, light microscopy, and histological analyses.

Materials and Methods

Cancer Model and Treatment

Nab-paclitaxel is a mitotic inhibitor used for treatment of breast, lung, pancreatic, and ovarian cancers [1,3]. Two types of human ovarian cancer cell line, OVCAR-8 and NCI/ADR-RES, were used in the current study. It has been reported that Nab-paclitaxel mitigates/reverses the development of OVCAR-8 tumors by slowing/blocking mitosis and inducing apoptosis, whereas NCI/ADR-RES is resistant to Nab-paclitaxel [26].

In Vitro Experiments

Cell Preparation. Human ovary carcinoma cell lines (OVCAR-8) were purchased from American Type Culture Collection (Manassas, VA), and the drug-resistant counterpart NCI/ADR-RES was obtained from the Drug Development Program at National Cancer Institute, and cultured in RPMI Medium 1640 supplemented with 10% FBS, 50 U/ml of penicillin, and 50 g/ml of streptomycin (Invitrogen, CA) under standard culture conditions in a humidified incubator maintained at 5% CO_2 and 37°C. OVCAR-8 and NCI/ADR-RES cells were cultured in 60-mm dishes to full confluence and then treated with either PBS or nab-paclitaxel at two different concentrations (100 and 500 nM) for 24 hours. All the cells were harvested by trypsinization, washed with PBS buffer, and resuspended with PBS/0.1% BSA. In MR experiments, cells were fixed with 4% paraformaldehyde in PBS for over 2 hours. After fixation, cells were washed, and approximately 35 million cells were centrifuged at 2000*g* × 2 minutes in a 0.65-ml of Eppendorf tube to obtain a tight cell pellet. All the liquid on the top was carefully removed, and the tube with cell pellet was used for MRI experiments. In flow cytometry experiments, cells were fixed with 3× volume of cold (−20°C) absolute ethanol and kept at −20°C. Before flow cytometry analysis (FACS), the cells were spun down and washed twice with PBS, resuspended with propidium iodide (PI) staining solution (3.8 mM sodium citrate, 50 μg/ml of PI, 0.5 mg/ml of RNase A in PBS) to a final cell concentration about 1×10^6 cell/ml, and incubated 3 or more hours at 4°C before FACS analysis. Samples were analyzed on a flow cytometer FACSCalibur (BD Biosciences, Mountain View, CA) with a minimum of 10,000 cells analyzed per sample. The data were collected with CellQuest software (BD Biosciences) and analyzed with Matlab R2013b.

NMR Measurements In Vitro. All measurements were performed on a Varian DirectDrive horizontal 4.7-T magnet (Varian Inc., Palo Alto, CA) equipped with a self-shielded SGRAD 115/60/S gradient system (Magnex Scientific Limited, Yarnton, Oxford, UK). A 40-mm inner diameter millipede volume coil was used for RF transmission and reception. As described above, OVCAR-8 and NCI/ADR-RES cells were treated with three different concentrations of Nab-paclitaxel with four samples at each concentration. ADC values for both conventional DWI (using a pulsed gradient spin echo [PGSE] sequence) as well as for TDS (using an oscillating gradient spin echo [OGSE] acquisition) were measured. Two gradient *b* values (0 and 400 s/mm^2) were used in both PGSE and OGSE measurements. The OGSE pulse sequence used two apodized cosine-modulated gradients as described in references [21,27]. For PGSE experiments, diffusion gradient durations were δ = 4 milliseconds and separation Δ = 48 milliseconds. The OGSE measurements were made using gradient frequencies from 50 to 350 Hz with an interval of 50 Hz. Note that the echo times (echo time = 67 milliseconds) for both PGSE and OGSE measurements were the same to minimize relaxation effects.

In Vivo Experiments

Animals and Tumor Induction. All procedures were approved by our Institutional Animal Care and Usage Committee at Vanderbilt University. Female Athymic nude mice (Harlan Laboratories, Inc., Indianapolis, IN) were used for the study and observed daily and weighed weekly to ensure that interventions were well tolerated.

Experiment Outline. Because the current study focuses on ovarian cancer, only female athymic nude mice were used. Twelve mice were inoculated with OVCAR-8 cells into the right hind limb, and 10 mice were inoculated with NCI/ADR-RES cells. When a tumor reached a size of 200 to 300 mm^3, the mouse underwent pretreatment MRI scans followed by the first treatment. This time point was defined as day 0. The 12 OVCAR-8 tumor-bearing mice were treated with either Nab-paclitaxel (n = 7) or drug vehicle PBS (n = 5) every other day at 15 mg/kg for 4 days. The 10 NCI/ADR-RES tumor-bearing mice were treated with either Nab-paclitaxel (n = 5) or PBS (n = 5) every other day at 15 mg/kg for 4 days. The injection of drug or drug vehicle was administered by a single intraperitoneal injection. Each treated mouse with either Nab-paclitaxel or PBS was imaged at pretreatment on day 0 and after two treatments on day 4, and was sacrificed for collection of tumor tissues immediately after the second imaging time point.

In Vivo MR Imaging. Animals were anesthetized with a 2%/98% isoflurane/oxygen mixture before and during scanning, and the magnet bore temperature was kept at 32°C using a warm-air feedback system. Stretchable medical tapes were used to ensure the proper positioning of hind limbs and tumors and to restrain movement caused by respiration, as well as to reduce motion-induced artifacts in the image data. Respiratory signals were monitored using a small pneumatic pillow placed under the mouse abdomen, and respiration gating (SA Instruments, Stony Brook, NY) was applied to further reduce motion artifacts. A doped water phantom (5 mM $CuSO_4$) was placed beneath the animal at thermal equilibrium with the magnet bore temperature, and its ADC value was measured to monitor the consistency of ADC measurements. The details of animal settings have been reported previously [22].

Both OGSE and PGSE sequences were implemented using a two-shot echo planar imaging acquisition using the same MRI equipment as described above. The imaging parameters were as follows: for PGSE experiments, diffusion gradient durations were δ = 4 milliseconds and separation Δ = 48 milliseconds. The OGSE sequence used gradient frequencies from 50 to 350 Hz with δ/Δ = 20/25 milliseconds, corresponding to effective diffusion times approximately from 5 to 0.7 milliseconds. Two *b* values (0 and 400 s/mm^2) were used for both PGSE and OGSE acquisitions. Multiple axial slices covering the entire tumor were acquired with a slice thickness of 2 mm. The matrix size was 128 × 64 with field of view = 40 × 20 mm, yielding an isotropic in-plane resolution of 312.5 μm. Note that the echo times (echo time = 67 milliseconds) for all ADC measurements were again the same to minimize relaxation effects. In addition, multiple axial slices, T2-weighted images covering the same volume as ADC measurements were collected with the following parameters: time to repetition = 4 seconds; time to echo = 0.05 seconds; slice thickness = 2 mm; the matrix size was 128 × 64 with field of view = 40 × 20 mm.

Histology. All the animals were sacrificed immediately after the last MRI session. The tumors were then dissected, cut into small pieces of approximately 2 mm in thickness, and immersed in formalin for 24 hours. All the tumor tissues were embedded in paraffin. To quantify mitotic index, proliferation, and apoptosis, three single, 8-μm-thick tissue sections were taken from each piece of tissue and stained with anti-phosphohistone H3 (PHH3), Ki-67 antibody, and caspase-3 antibody, respectively, according to standard protocols of the manufacturer's manual. All the stained slides were scanned by a Leica SCN400 Slide Scanner with a magnification of 20 to generate high-resolution digital images. A purpose-written segmentation algorithm was implemented to calculate percentages of caspase-3–activated area and Ki-67–positive cells, mitotic index (the number of PHH3-positive cells divided by the number of total cells), and

cellularity (the number of total cells divided by the total area of tissue) for the entire slides.

Diffusion Models and Data Analysis. Tumor volumes were calculated from T2-weighted Images. As only two imaging time points 4 days apart were selected, central tumor necrotic cores (defined by very high T2W MR signals, high ADC values, and flat ADC spectra independent on frequencies due to the high water content) were only found in a few tumors. These necrotic cores were excluded from the diffusion and histology analyses to better characterize the treatment response of viable tumor tissues.

The ADC values were then calculated for the nonnecrotic tumor region on each slice using Eq. (1):

$$ADC = -\log\left(\frac{I(b_2 = 400)}{I(b_1 = 0)}\right)/(b_2 - b_1) \quad (1)$$

Here $I(b)$ is the diffusion-weighted signal intensity with a specific b value (here, 0 or 400 s/mm^2).

If tumors are assumed to consist of impermeable spherical cells, the analytical expression of ADC values for TDS diffusion measurements is given by:

$$ADC_{sphere}(f) = \frac{8\pi^2 f^2}{\delta}\sum_n \frac{B_n\lambda_n^2\left(D_{inf} - D_0\right)^2}{\left(\lambda_n^2\left(D_{inf} - D_0\right)^2 + 4\pi^2 f^2\right)^2} \times \left\{\frac{\left(\lambda_n^2\left(D_{inf} - D_0\right)^2 + 4\pi^2 f^2\right)}{\lambda_n D_{in}}\left[\frac{\delta}{2} + \frac{sin(4\pi f\delta)}{8\pi f}\right] - 1 + exp\left(-\lambda_n\left(D_{inf} - D_0\right)\delta\right) + exp\left(-\lambda_n\left(D_{inf} - D_0\right)\Delta\right) \times \left(1 - cosh\left(\lambda_n\left(D_{inf} - D_0\right)\delta\right)\right)\right\} \quad (2)$$

f is the oscillation frequency, δ is the gradient duration, Δ is the separation of two diffusion gradients. The terms B_n and λ_n are structure-dependent parameters that depend on sphere diameters [21]. The accuracy of Eq. (2) has been validated by computer simulations [21] and phantom experiments [28]. Note that the ADC represented by Eq. (2) drops to zero at long diffusion times or low frequencies (i.e., $ADC_{sphere}[f = 0] = 0$) because of complete restriction. However, in biological tissues, the presence of permeable cell membranes and the nature of the extracellular space tortuosity lead to a nonzero value for $ADC_{sphere}(f = 0)$. To count for these effects, a modified tumor ADC model was used as

$$\mathrm{ADC}_{tumor}(f) = \mathrm{ADC}_{sphere}\left(f, d, D_{inf} - D_0\right) + D_0 \quad (3)$$

where D_{inf} and D_0 represent the tumor ADC values at infinitely high and zero frequencies, respectively. The mean ADC spectra of the tumor region on each slice were fit to the Eq. (3). The restriction size d represents the mean restriction dimension in tumors, which is associated with mean tumor cell size because cell membranes have been reported as the dominant restriction barriers in tissues [29]. In tumor tissues, D_0 and D_{inf} are mainly determined by the extracellular tortuosity [30] and intracellular diffusion coefficient, respectively.

Statistical Analysis

The differences in cell sizes derived from FACS and microscopy, and MR-derived measures of restriction among the different types of cell samples treated with Nab-paclitaxel at different concentrations (Figures 1–3) were summarized using means and standard deviations and compared by one-way analysis of variance (ANOVA). The differences in three fitted parameters from the TDS data (d, D_{inf}, and D_0) and conventional (PGSE-derived) ADC values for the two types of tumors treated with either PBS or Nab-paclitaxel (Figure 5) were summarized using means and standard deviations and compared by a Kruskal-Wallis test. All the tests were two-sided, and a false discovery rate (FDR)–adjusted P value of .05 or less was taken to indicate statistical significance. Statistical analyses were performed using Matlab R2013b.

Results

Flow Cytometry And Microscopy Analysis

Flow cytometry measures multiple physical characteristics of single cells as they flow in a fluid stream through a beam of light. Light scattering occurs when a single cell deflects incident laser light. The width of forward-scattered light (FSC-W) is proportional to cell size [31]. Figure 1*A* shows the distributions of FSC-W (sample size is 6100) for OVCAR-8 (responder) and NCI/ADR-RES (resistant) cells treated with various concentrations of Nab-paclitaxel (0, 100, and 500 nM). FSC-Ws for OVCAR-8 cells increase continuously as the concentration goes higher ($P < .0001$), indicating antimitotic treatment–induced increases in cell size. No significant differences ($P > .05$) in FSC-W are observed between PBS-treated and 100 nM Nab-paclitaxel–treated NCI/ADR-RES cells, whereas FSC-W of 500 nM Nab-paclitaxel–treated NCI/ADR-RES is significantly larger than the other two cohorts ($P < .0001$), indicating that NCI/ADR-RES is responsive only to a very high concentration of Nab-paclitaxel.

Flow cytometry also distinguishes cells in different phases of the cell cycle by quantifying different DNA contents they contain. The emission light intensity of PI-labeled cells is proportional to the amount of DNA present in the cells, and its histogram is used to calculate the percentage of cells in the different parts of the cell cycle [31]. The DNA content of G_2/M cells is about twice that of G_0/G_1 cells because the chromosomes have been doubled during S phase. Polypoid cells sometimes appear in cancer cells, which have more DNA content than G_2/M cells. DNA fragmentation is one of the hallmarks of apoptosis [32]. As a result, sub-G_0 cells are usually associated with apoptotic cells. As shown in Figure 1*C* and Supplementary Table 1, the percentages of G_2/M Nab-paclitaxel–treated OVCAR-8 cells continue to increase from 32% at 0 nM to 64.2% at 100 nM and to 76.3% at 500 nM, indicating a significant treatment-induced G_2/M phase arrest as expected. NCI/ADR-RES cells treated with 100 nM Nab-paclitaxel show a very slightly increase from 34% to 36.5% in the population of G_2/M cells. By contrast, NCI/ADR-RES cells treated with 500 nM Nab-paclitaxel exhibit a large population (62.2%) of G_2/M cells, again demonstrating that NCI/ADR-RES is more responsive to higher concentration of Nab-paclitaxel. It is also noted that populations of sub-G_0 cells associated with apoptotic cells are small for the cell samples that have significant mitotic arrest, suggesting that mitotic arrest may be the first cellular response to Nab-paclitaxel treatment.

The absolute cell sizes were measured by light microscope (Figure 1*B*, $n = 620$). The mean cell size of OVCAR-8 keeps increasing with increasing concentrations of Nab-paclitaxel ($P < .0001$), whereas the Nab-paclitaxel–treated NCI/ADR-RES cells swell measurably only at the concentration of 500 nM ($P = .004$).

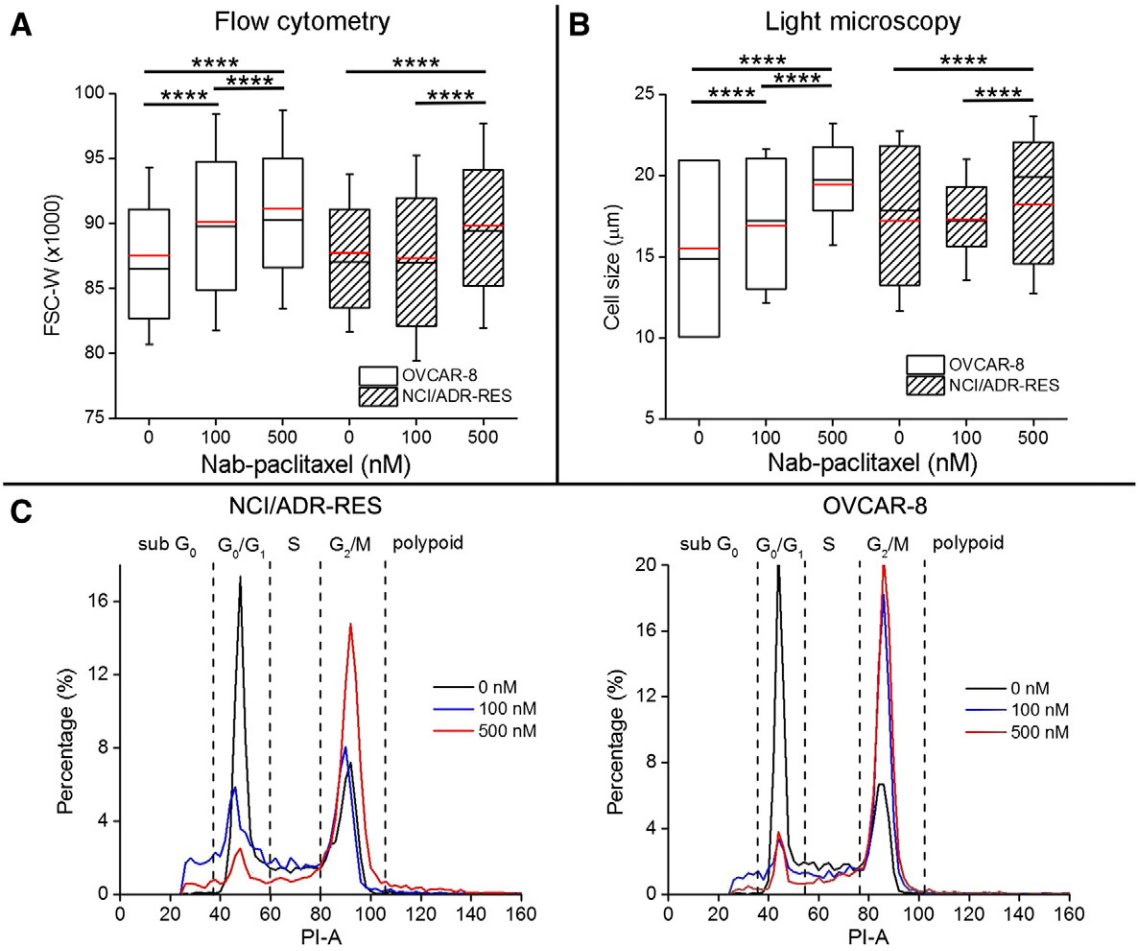

Figure 1. Cell size changes measured by flow cytometry and light microscopy and cell cycle analysis. (A) Box-and-whisker plots of the FSC-W for OVCAR-8 and NCI/ADR-RES treated with various concentrations of Nab-paclitaxel (0, 100, and 500 nM). The sample size of each cohort is 6100. (B) Box-and-whisker plots of the cell size measured by light microscopy for OVCAR-8 and NCI/ADR-RES treated with various concentrations of Nab-paclitaxel (0, 100, and 500 nM). The sample size of each cohort is 620. For all the box-and-whisker plots, the 25th to 75th percentiles are blocked by the boxp; the black and red bands inside the box are the median and mean, respectively; and the whiskers mark the SD. ****$P < .0001$ as measured by one-way ANOVA with an FDR posttest. (C) Histograms of the emission light intensity of PI-labeled NCI/ADR-RES and OVCAR-8 cells treated with Nab-paclitaxel at 0 (black line), 100 (blue line), and 500 nM (red line).

Nab-paclitaxel is used to trap cells in the M phase which then undergo apoptosis. It is known that cells significantly increase their sizes during the M phase. Here, our flow cytometry and light microscope analyses confirm that Nab-paclitaxel–treated OVCAR-8 cells undergo significant mitotic arrest and show increases in cell size in response to the antimitotic treatment.

Histological Analysis

Representative PHH3-stained slides for either Nab-paclitaxel or PBS-treated OVCAR-8 and NCI/ADR-RES tumors are shown in Supplementary Figure 2. The brown stain represents mitotic cells. The percentage of mitotic cells (the number of PHH3-positive cells divided by the total number of cells) is calculated from the high-resolution digital images of each PHH3-stained slide (Supplementary Figure 3). As shown in Figure 2*B*, Nab-paclitaxel–treated OVCAR-8 tumors have a significantly higher percentage of mitotic cells than PBS-treated OVCAR-8 tumors ($P = .04$). No significant difference is observed between Nab-paclitaxel– and PBS-treated NCI/ADR-RES tumors.

The percentage of caspase-3–activated area was calculated from the high-resolution digital images of each caspase-3–stained slide. Nab-paclitaxel–treated OVCAR-8 tumors have the highest percentage of caspase-3–activated area (~35%) among all the cohorts ($P = .04$), indicating treatment-induced apoptosis (Figure 2*C*).

Nab-paclitaxel–treated OVCAR-8 tumors have a lower average cellularity than PBS-treated OVCAR-8 tumors, but the difference is not significant (Figure 2*A*). There are no significant differences in percentages of Ki-67–positive cells between Nab-paclitaxel– and PBS-treated tumors (Figure 2*D*). Although some studies have reported increases in percentages of Ki-67–positive cells in paclitaxel-treated tumors [33,34], many other animal and human studies did not observe significant changes in proliferative activity as measured by Ki-67 in tumor tissues following paclitaxel [35–37]. A possible explanation is that the changes in Ki-67 expression are highly dependent on the choices of observation time points posttreatment.

Changes in Tumor Cell Size in Response to Antimitotic Treatment quantified by TDS Restriction Size In Vitro Experiments

The fitted mean restriction size of Nab-paclitaxel–treated OVCAR-8 cells increased significantly ($P = .04$) with increasing drug concentration (Figure 3*A*). By contrast, there were no significant changes in restriction size of Nab-paclitaxel–treated NCI/ADR-RES

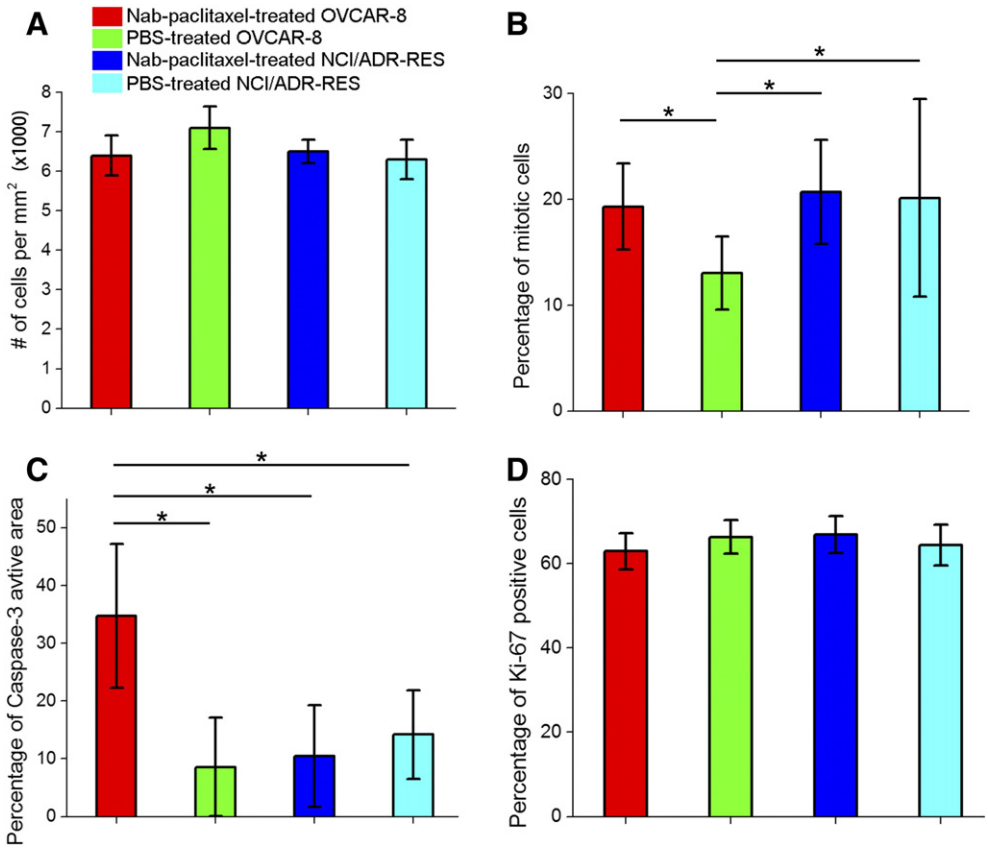

Figure 2. Cellularity (A), percentages of mitotic cells (B), caspase-3–activated area (C), and percentages of Ki-67–positive cells (D) for Nab-paclitaxel–/PBS-treated OVCAR-8 and NCI/ADR-RES tumors. *$P < .05$ as measured by one-way ANOVA with an FDR posttest.

cells ($P > .05$). The increase in restriction size for Nab-paclitaxel–treated OVCAR-8 cells reflects the increase of tumor cell size in response to antimitotic treatment, which is confirmed by 1) changes in mean cell size measured by light microscopy (Figure 1*B*) and 2) changes in the FSC-W measured by flow cytometry (Figure 1*A*). Differences in restriction size between PBS-treated NCI/ADR-RES and OVCAR-8 cells as shown in Figure 3*A* may result from the intrinsic differences in cell size between different types of cells. The absolute cell sizes are reported to be 16.07 ± 2.42 μm and 14.24 ± 2.71 μm for NCI/ADR-RES and OVCAR-8 cells [38,39], respectively.

Figure 3*B* shows that the fitted D_{inf} of 500 nM Nab-paclitaxel–treated OVCAR-8 cells is significantly lower than that of PBS-treated OVCAR-8 cells ($P = .04$), likely because of the increased structural complexity inside arrested cells in M phase. The fitted D_0 of Nab-paclitaxel–treated OVCAR-8 cells (Figure 3*C*) shows a decreasing trend as the drug concentration increases. The fitted D_0 and PGSE-derived ADC of 100 nM Nab-paclitaxel–treated NCI/ADR-RES cells are significantly lower than those of PBS-treated NCI/ADR-RES cells ($P < .05$). These decreases in either D_0 or PGSE-derived ADC indicate a decreased tortuosity of the extracellular space. In our cell experiment, all the cells were treated firstly with either PBS or Nab-paclitaxel and then centrifuged to create tight cell pellets with the same speed and time. Morphological properties of the extracellular space depend on how the cells are arranged during centrifugation and may correlate with the cell size distribution. As shown in Figure 1*C*, two types of cells treated with the same concentration of Nab-paclitaxel have similar DNA content distribution, which is roughly the same as the cell volume distribution. Interestingly, the D_0 and PGSE-derived ADC values for OVCAR-8 and NCI/ADR-RES treated with the same concentration of Nab-paclitaxel are almost the same. Although the cell pellet is not an appropriate system to investigate the treatment-induced changes in tortuosity of the extracellular space, it fulfills our purpose to measure the treatment-induced changes in cell size.

In Vivo Experiments

Figure 4*A* shows ADC maps of a representative slice obtained using TDS at frequencies ranging from 0 to 350 Hz overlaid on the corresponding T2-weighted images. ADC values for the tumor region increase as the frequency increases, indicating less restrictions to water molecules at higher frequencies or shorter diffusion times. Meanwhile, ADC values for the water phantom do not change with the frequency, confirming that the ADC changes in tumor are not an instrument artifact. The ADC changes for an OVCAR-8 tumor before and after a 4-day Nab-paclitaxel treatment are quantitatively shown in Figure 4*B*. A typical ADC spectrum for tumor is characterized by a low ADC value at zero frequency followed by a rapid increase that reaches a plateau, quantified by three spectral parameters D_0, d, and D_{inf}, respectively. The three parameters for nontreated and Nab-paclitaxel–treated OVCAR-8 are $d = 5.92$ μm, $D_{inf} = 1.58$ μm^2/ms, and $D_0 = 0.47$ μm^2/milliseconds and $d = 9.22$ μm, $D_{inf} = 1.36$ μm^2/ms, and $D_0 = 0.37$ μm^2/milliseconds, respectively. The increase of d from 5.92 to 9.22 μm reflects the treatment-induced increase in tumor cell size.

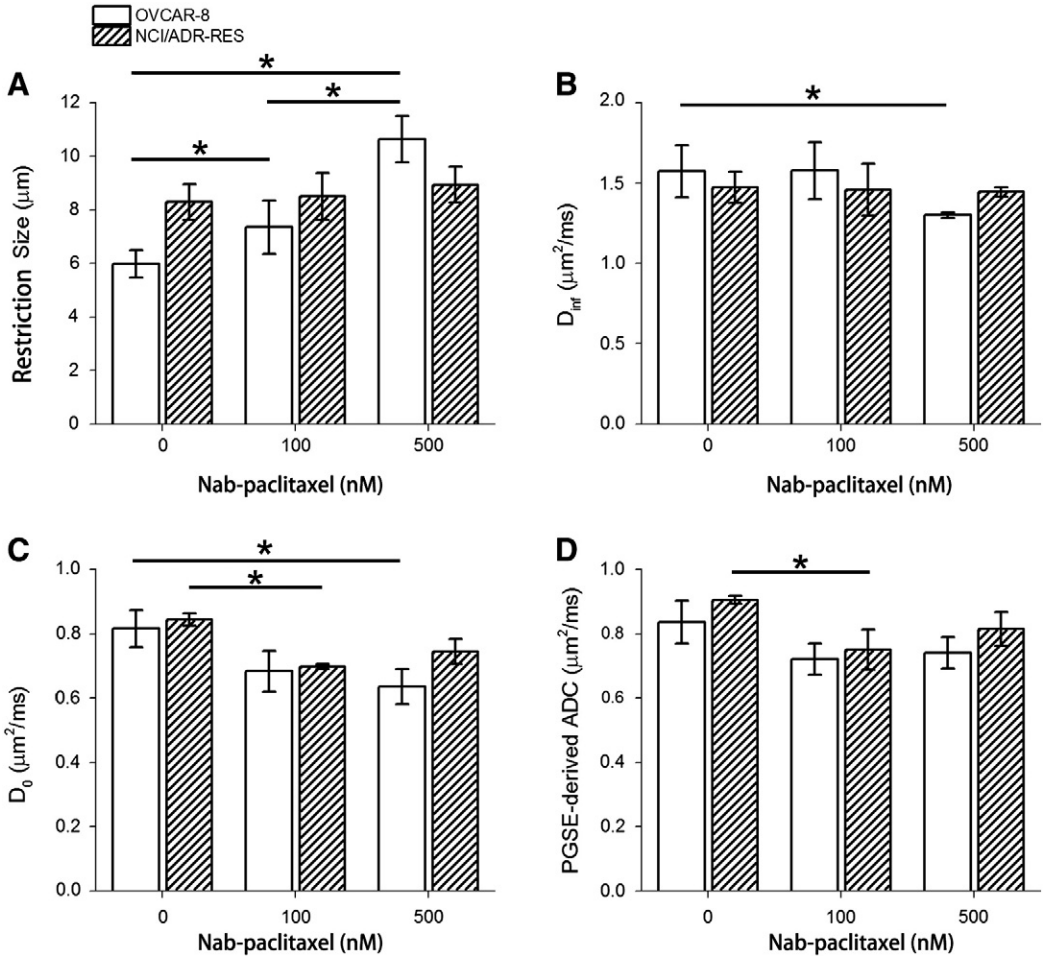

Figure 3. Fitted d (A), D_{inf} (B), D_0 (C), and PGSE-derived ADC (D) for OVCAR-8 and NCI/ADR-RES cell pellets treated with Nab-paclitaxel at 0, 100, and 500 nM. *$P < .05$ as measured by one-way ANOVA with an FDR posttest.

Supplementary Figure 4 shows that there are no significant ($P > .05$) differences in tumor growth among PBS/Nab-paclitaxel–treated tumors. Figure 5 summarizes the percentage changes before and after PBS/Nab-paclitaxel treatments in the fitted spectral parameters and PGSE-derived ADC for all the tumors. Six of seven Nab-paclitaxel–treated OVCAR-8 tumors show an increase (>20%) of fitted mean

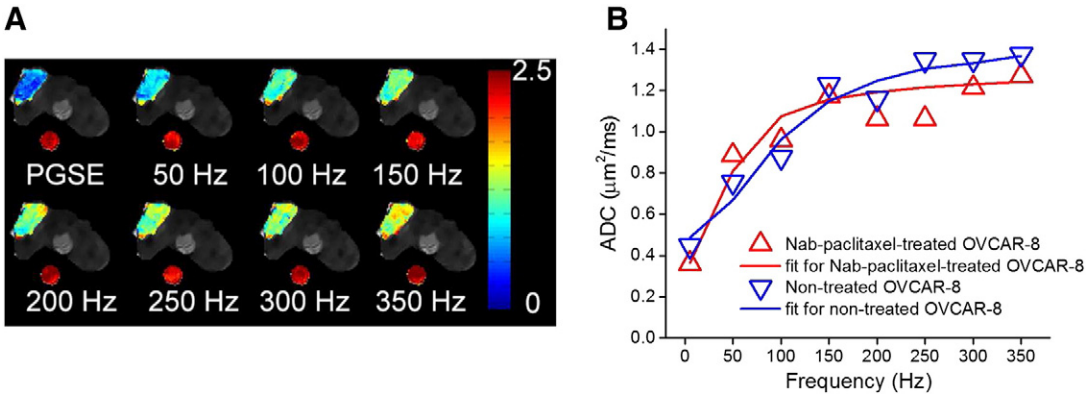

Figure 4. (A) ADC maps of a representative slice through tumor and a water phantom at frequencies ranging from 0 to 350 Hz, overlaid on T2-weighted MR images. The water phantom was placed beneath the mouse to monitor the accuracy and consistency of ADC measurements. (B) Representative ADC values of an OVCAR-8 tumor at day 0 (nontreated) and day 4 (Nab-paclitaxel–treated) obtained using TDS and conventional PGSE acquisitions at frequencies ranging from 0 to 350 Hz. Solid lines represent the fits using Eqs. (1) to (3). The fitted parameters for nontreated (blue) and Nab-paclitaxel–treated (red) OVCAR-8 are $d = 5.92\,\mu m$, $D_{inf} = 1.58\,\mu m^2/ms$, and $D_0 = 0.47\,\mu m^2/ms$ and $d = 9.22\,\mu m$, $D_{inf} = 1.36\,\mu m^2/ms$, and $D_0 = 0.37\,\mu m^2/ms$, respectively. It is noted that the ADC measured using PGSE with a diffusion time of 48 milliseconds is plotted as the ADC at a corresponding frequency of 5.2 Hz.

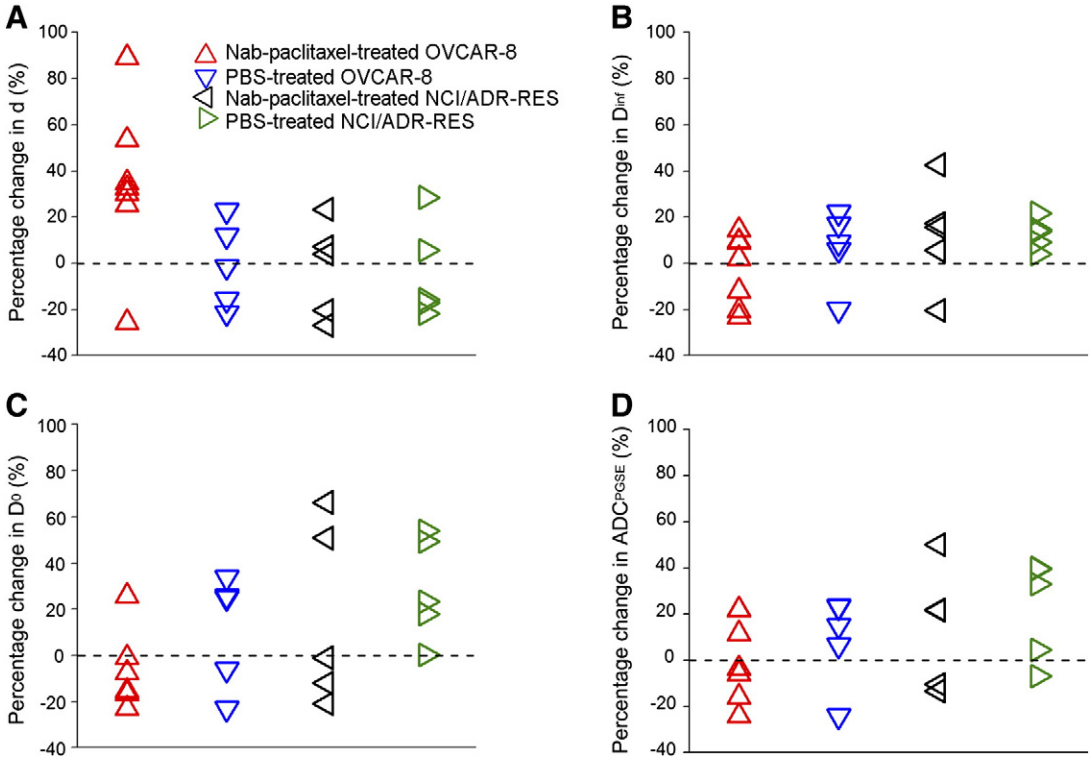

Figure 5. Percentage changes in d (A), D_{inf} (B), D_0 (C), and PGSE-derived ADC (D) for OVCAR-8 and NCI/ADR-RES tumors receiving a 4-day treatment of either Nab-paclitaxel or PBS at a dose of 15 mg/kg.

restriction size d (Figure 5*A*), which is significantly higher ($P = .05$) than that of the other three cohorts and consistent with our *in vitro* observations. These six Nab-paclitaxel–treated OVCAR-8 tumors also show a decrease of fitted D_0 (Figure 5*C*), indicating a decrease of extracellular volume due to the increase of cell size. Interestingly, there is one Nab-paclitaxel–treated OVCAR-8 tumor that showed a ~25% decrease of mean restriction size and a ~20% increase of D_0. It is also notable that this tumor had the largest percentage of caspase-3–activated area (65%) in all the treated-responder tumors. A possible explanation is that the tumor reached a later stage of pathological response to treatment so that most cells underwent apoptosis. The cell shrinkage during apoptosis may have overcome any increase in cell size that resulted from mitosis inhibition as illustrated in Supplementary Figure 1. There were no significant differences in the fitted D_{inf} and PGSE-derived ADC among two types of tumors treated with either Nab-paclitaxel or PBS ($P > .05$).

Figure 6 is a scatter plot of the percentages of changes in two spectral parameters (restriction size d and D_0) for all the animals. Two perpendicular axes (percentage change of $D_0 = 0$, $d = 20\%$, respectively) divide the plane into four areas. Six of seven Nab-paclitaxel–treated OVCAR-8 tumors and one of five Nab-paclitaxel–treated NCI/ADR-RES tumors are inside the bottom-right quadrant which has a decreased D_0 and >20% increase of d. The one Nab-paclitaxel–treated OVCAR-8 tumor which is not inside the bottom-right quadrant had the largest region undergoing apoptosis, a later effect of the treatment, among the Nab-paclitaxel–treated OVCAR-8 tumors. The one Nab-paclitaxel–treated NCI/ADR-RES tumor which is inside the bottom-right quadrant had the largest region undergoing apoptosis among the Nab-paclitaxel–treated NCI/ADR-RES tumors, suggesting that it may start to respond to the treatment. Therefore, a combination of decreased D_0 and increase of d may be an early indicator of effective antimitotic therapies.

Discussion

Reliable and sensitive methods for assessing the response of tumors to antimitotic therapies, a widely used treatment option for various cancers, are critical to minimize unnecessary toxicity and treatment

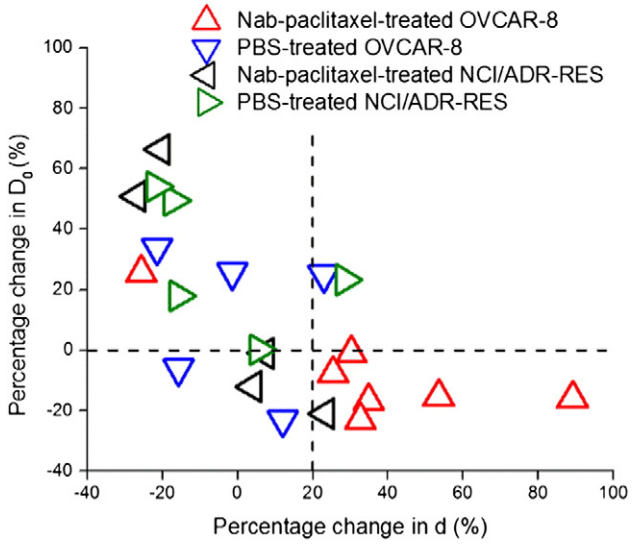

Figure 6. Scatter plot of the percentages of change in two spectral parameters (restriction size d and D_0) for all the treated tumors.

delays for switching to alternative more efficient treatment regimens at an early stage of treatment, and are also valuable for assisting the development of new drugs that inhibit mitosis. Mitotic arrest is a natural biomarker of tumor response to antimitotic therapy, but currently, it can be characterized only by scoring histology sections or stained biopsies in human and rodent cancer models. In this paper, TDS, combining a single long diffusion time conventional PGSE acquisition with a series of OGSE measurements, is demonstrated to quantify microstructural changes (notably, increases in cell size) in tumors as an early response marker for antimitotic therapy. The increases in cell size quantified by restriction size *d*, one of the spectral parameters derived from TDS measurements, occur when no significant changes in either cellularity (Figure 2*A*) or tumor volume regression (Supplementary Figure 4) are observed. Flow cytometry, light microscopy, and histological analyses correlate these increases in cell size with treatment-induced mitotic arrest. In addition, the combination of restriction size and D_0, a spectral parameter associated with tissue cellularity, is shown to distinguish the Nab-paclitaxel–treated responsive tumors from either Nab-paclitaxel–treated resistant tumors or PBS-treated responsive tumors, indicating TDS as a potential imaging marker for early detection of successful antimitotic therapies.

The concentrations of Nab-paclitaxel used in the cell experiment were 100 and 500 nM, at which the effects of paclitaxel on mitosis in culture are well understood [40]. Mitotic arrest increases cell size, whereas cell death is often coupled with a decrease of cell size. Our *in vitro* data, including flow cytometry, light microscopy, and TDS analyses, all detected an increase in cell size for OVCAR-8 cells treated with Nab-paclitaxel for 24 hours, consistent with 1) our cell cycle analysis indicating a significant G_2/M phase arrest and 2) a reported finding that cells at saturating paclitaxel concentrations (typically > 100 nM) rarely die without first entering mitotic arrest that can last 24 hours or longer depending on the cell line [40].

For our *in vivo* treatment study, a moderate dosing scheme (15 mg/kg, every other day) was chosen and demonstrated significant mitotic arrest and apoptosis induction in responsive tumors (Figure 3). Although cell shrinkage is one of the hallmarks in cell morphologic changes during apoptosis and may overcome the increase in cell size resulted from mitotic arrest, it occurs rather late in apoptosis. In the experiment, six of seven Nab-paclitaxel–treated OVCAR-8 tumors showed an increase (>20%) of fitted mean restriction size *d*. There is one Nab-paclitaxel–treated OVCAR-8 tumor which had the largest percentage of caspase-3–activated area (65%) in all the treated-responder tumors; it showed a ~25% decrease of mean restriction size. This implies that mitotic arrest is the first cellular response to antimitotic therapies, followed by apoptosis, consistent with previous findings. Increases in cell size dominate the overall imaging results for responsive tumors that have not reached a later stage of pathological response to treatment. Therefore, TDS method is reliable to detect mitosis arrest at early stages of response to antimitotic therapies. In addition, TDS method may provide a comprehensive means to monitor temporal dynamic changes of tumor status following treatment.

A single ADC value measured with a relatively long diffusion time has been shown to negatively correlate with cellularity and has previously been used to monitor tumor response to therapy [9,14,41]. However, our PGSE-derived ADC values with a diffusion time of 48 milliseconds do not differentiate the Nab-paclitaxel–treated responsive tumors from PBS-treated responsive tumors and PBS/Nab-paclitaxel–treated resistant tumors. The histological data showed that the Nab-paclitaxel–treated responsive tumors have a lower mean cellularity than the PBS-treated responsive tumors, but the difference is not significant. In addition, ADC values are affected by multiple microstructural features simultaneously not limited to cellularity. The increases in cell size that resulted from mitotic arrest reduce the extracellular spaces and thus decrease the PGSE-derived ADC values, which may compromise the increase in ADC values due to cell loss. Therefore, the conventional measurements of a single averaged ADC at a long diffusion time may not be specific enough to characterize accurate pathologic changes in tumors following treatments, which in turn decreases the sensitive to assess the early therapeutic response of tumors. By contrast, the proposed TDS method enhances the specificity of DW-MRI to specific cellular changes such as cell size, which in turn provides a means to assess tumor status more accurately following treatments.

Our *in vitro* results show that the fitted restriction sizes are significantly smaller (~50%) than cell sizes measured by light microscope for the same type of cell line receiving the same treatment. This discrepancy is not too surprising, as the simplified model assumes spherical cells or a single size parameter. Moreover, cells observed by light microscope float on a drop of PBS solution without pressure from neighboring cells. By contrast, cells in tumors are tightly packed which may reduce the extent of cell swelling during mitosis arrest. Secondly, the restriction size characterizes the mean length scale of the restrictions in biological tissues. In tumors, the cells are tightly packed, and accordingly, the restriction size should be dominated by cell size. However, pathway lengths in extracellular spaces, which are much smaller than cell sizes, also contribute to the derived restriction size and may average down the estimated restriction dimension. A more complex two-compartment model for fitting diffusion spectra has been proposed to extract mean cell size as well as intracellular volume fraction. It has proven successful in well-characterized cell cultures [42] and fixed tissues [43]. It may provide an accurate way to measure cell size in further *in vivo* treatment studies, but this more accurate approach requires longer scanning times with multiple *b* values compared with the current approach.

The range of diffusion times or gradient frequencies used in TDS determines the length scales of the structural variations to which the method is sensitive. The measured ADC is able to probe finer structural changes as the effective diffusion time becomes shorter or the frequency becomes higher. But acquiring diffusion-weighted signals at very high frequency needs very high gradient strengths. For example, a gradient strength of 68 G/cm, much higher than the maximum gradient strength applicable in current clinical settings, was used in our study to measure ADC at 350 Hz. Fortunately, our MR findings indicate that the restriction size and D_0 are more valuable than D_{inf} in detecting structural changes in response to antimitotic therapies. The restriction size characterizes how ADC rises in response to an increase in the frequency and D_0 represents the ADC at very low frequency. As reported in our previous cell size measurement study, the rising portion of ADC spectra almost ends before the frequency reaches 150 Hz for cells with size from 5 to 20 μm, covering the cell size range of most solid tumors. Therefore, the current acquisition scheme of TDS can be optimized by reducing the highest frequency (for example, from 350 Hz to 150 Hz) if tumor cell size is the primary target for monitoring treatment response. It will significantly lower the maximum gradient strength required and

shorten the total scan time, thereby improving the likelihood of effective clinical translation.

The location of tumor formation is relevant in mimicking human diseases. The subcutaneous xenograft model of ovarian cancer used in this paper provides a platform to verify the feasibility of TDS imaging method in detecting treatment-induced mitotic arrest noninvasively. Note that this model is not ideal for survival studies determining the efficacy of therapies. Either intraperitoneal or orthotopic xenograft model has been suggested to better mimic various stages of ovarian cancer and is useful to investigate the influences of treatments on survival rates [44]. However, this is out of the main scope of the current work that focuses on the development and validation of a novel imaging method for detection of mitosis arrest. In the future studies, it is interesting to investigate performance of TDS method in assessing therapeutic response using either an intraperitoneal or orthotopic xenograft mouse model.

Microcirculatory perfusion of blood within capillaries was assumed negligible in the current study. This assumption has been used in many treatment studies using DW-MRI [16,9] because the perfusion fraction of tissues is usually much smaller than the diffusion fraction of tissues. In cases where effects that resulted from tumor angiogenesis on ADC measurements cannot be assumed negligible, the current PGSE/OGSE sequences can be modified to acquire perfusion-free MR signals by inserting a PGSE filter with a small b value at the beginning of the sequence [45].

In this proof-of-concept study, TDS is shown to provide an *in vivo* detection of mitotic arrest which is an early cellular marker for antimitotic therapies. Therefore, TDS may assist to investigate many critical questions regarding antimitotic therapies. For example, the dose-dependent effects of antimitotic drugs on cell biology *in vivo* [17,18] and how the cellular responses correlate with therapeutic outcome are not fully understood. Profiling the time course changes in TDS-derived restriction size d in response to treatments with multiple dosing schemes may provide more insights into these questions. It should be emphasized that applications of TDS are not limited in antimitotic therapies only. Based on its capability of measuring specific cellular morphologic changes, this method can be useful in characterizing tumor response to other therapies which induce microstructural variations in tumor tissues. For example, it has been reported that cell swelling is the first manifestation of various chemo/radiotherapy-induced cell injuries [14,15]. Also, cell shrinkage is a typical feature of apoptosis, which is a common target for many anticancer therapies [46,47]. A recent study reported *in vitro* detection of apoptosis by measuring ADC values of normal and apoptotic cells at a broad range of effective diffusion times [48]. Therefore, TDS may have a wide array of applications for detecting tumor response to various therapies and greatly enhance the specificity of MRI methods in the evaluation of therapeutic response.

Conclusion

In the work reported herein, a novel MRI-based approach to assessing tissue water diffusion over varying time scales was used to examine the cellular response to Nab-paclitaxel in culture and human ovarian cancer xenografts. The Nab-paclitaxel–induced increase in cell size was observed using flow cytometry and light microscopy in cultured cells. Histological analyses confirmed that Nab-paclitaxel induces mitotic arrest and apoptosis in tumors. Both *in vitro* and *in vivo* MR data obtained using TDS demonstrated that the restriction size d obtained from ADC spectra is able to quantify the increase in cell size associated with mitotic arrest and multinucleation. Moreover, the combination of restriction size and D_0 is shown to distinguish the Nab-paclitaxel–treated responsive tumors from either Nab-paclitaxel–treated resistant tumors or PBS-treated responsive tumors, indicating TDS as a potential imaging marker in early detection of successful antimitotic therapies. Conventional DW-MRI using PGSE sequences was also implemented in the study for detecting treatment response. However, the ADC at diffusion time = 48 milliseconds, a common value used in PGSE acquisitions, does not differentiate the Nab-paclitaxel–treated responsive tumors from PBS-treated responsive tumors and PBS/Nab-paclitaxel–treated resistant tumors.

Supplementary data to this article can be found online at http://dx.doi.org/10.1016/j.neo.2016.04.006.

Authors' Contributions

Conception and design: X. Jiang, H. Li, J. Xu, J. C. Gore

Development of methodology: X. Jiang, H. Li, J. Xu, J. C. Gore

Acquisition of data (provided animals, acquired and managed patients, provided facilities, etc.): X. Jiang, P. Zhao, J. Xie, D. Khabele

Analysis and interpretation of data (e.g., statistical analysis, biostatistics, computational analysis): X. Jiang, H. Li, J. Xu

Writing, review, and/or revision of the manuscript: X. Jiang, H. Li, P. Zhao, J. Xie, D. Khabele, J. Xu, J. C. Gore

Administrative, technical, or material support (i.e., reporting or organizing data, constructing databases): J. Xu, J. C. Gore

Study supervision: J. C. Gore

Grant Support

This study has been supported by National Institutes of Health grants R01CA109106 (to J. C. Gore) and R01CA173593 (to J. C. Gore).

References

[1] Jordan MA and Wilson L (2004). Microtubules as a target for anticancer drugs. *Nat Rev Cancer* **4**, 253–265.

[2] Wang TH, Wang HS, and Soong YK (2000). Paclitaxel-induced cell death: where the cell cycle and apoptosis come together. *Cancer* **88**, 2619–2628.

[3] Green MR, Manikhas GM, Orlov S, Afanasyev B, Makhson AM, Bhar P, and Hawkins MJ (2006). Abraxane, a novel Cremophor-free, albumin-bound particle form of paclitaxel for the treatment of advanced non–small-cell lung cancer. *Ann Oncol* **17**, 1263–1268.

[4] Duffaud F and Therasse P (2000). New guidelines to evaluate the response to treatment in solid tumors. *Bull Cancer* **87**, 881–886.

[5] Weber WA (2009). Assessing tumor response to therapy. *J Nucl Med* **50**(Suppl. 1), 1S–10S.

[6] Michaelis LC and Ratain MJ (2006). Measuring response in a post-RECIST world: from black and white to shades of grey. *Nat Rev Cancer* **6**, 409–414.

[7] Symmans WF, Volm MD, Shapiro RL, Perkins AB, Kim AY, Demaria S, Yee HT, McMullen H, Oratz R, and Klein P, et al (2000). Paclitaxel-induced apoptosis and mitotic arrest assessed by serial fine-needle aspiration: implications for early prediction of breast cancer response to neoadjuvant treatment. *Clin Cancer Res* **6**, 4610–4617.

[8] Avril N, Sassen S, Schmalfeldt B, Naehrig J, Rutke S, Weber WA, Werner M, Graeff H, Schwaiger M, and Kuhn W (2005). Prediction of response to neoadjuvant chemotherapy by sequential F-18-fluorodeoxyglucose positron emission tomography in patients with advanced-stage ovarian cancer. *J Clin Oncol* **23**, 7445–7453.

[9] Thoeny HC and Ross BD (2010). Predicting and monitoring cancer treatment response with diffusion-weighted MRI. *J Magn Reson Imaging* **32**, 2–16.

[10] Hamstra DA, Rehemtulla A, and Ross BD (2007). Diffusion magnetic resonance imaging: a biomarker for treatment response in oncology. *J Clin Oncol* **25**, 4104–4109.

[11] Moffat BA, Chenevert TL, Meyer CR, McKeever PE, Hall DE, Hoff BA, Johnson TD, Rehemtulla A, and Ross BD (2006). The functional diffusion map: an imaging biomarker for the early prediction of cancer treatment outcome. *Neoplasia* **8**, 259–267.

[12] Chenevert TL, McKeever PE, and Ross BD (1997). Monitoring early response of experimental brain tumors to therapy using diffusion magnetic resonance imaging. *Clin Cancer Res* **3**, 1457–1466.

[13] Galons JP, Altbach MI, Paine-Murrieta GD, Taylor CW, and Gillies RJ (1999). Early increases in breast tumor xenograft water mobility in response to paclitaxel therapy detected by non-invasive diffusion magnetic resonance imaging. *Neoplasia* **1**, 113–117.

[14] Patterson DM, Padhani AR, and Collins DJ (2008). Technology insight: water diffusion MRI—a potential new biomarker of response to cancer therapy. *Nat Clin Pract Oncol* **5**, 220–233.

[15] Moffat BA, Chenevert TL, Lawrence TS, Meyer CR, Johnson TD, Dong Q, Tsien C, Mukherji S, Quint DJ, and Gebarski SS, et al (2005). Functional diffusion map: a noninvasive MRI biomarker for early stratification of clinical brain tumor response. *Proc Natl Acad Sci U S A* **102**, 5524–5529.

[16] Galban CJ, Hoff BA, Chenevert TL, and Ross BD (2016). Diffusion MRI in early cancer therapeutic response assessment. *NMR Biomed*. http://dx.doi.org/10.1002/nbm.3458 [Epub ahead of print].

[17] Orth JD, Kohler RH, Foijer F, Sorger PK, Weissleder R, and Mitchison TJ (2011). Analysis of mitosis and antimitotic drug responses in tumors by in vivo microscopy and single-cell pharmacodynamics. *Cancer Res* **71**, 4608–4616.

[18] Milross CG, Mason KA, Hunter NR, Chung WK, Peters LJ, and Milas L (1996). Relationship of mitotic arrest and apoptosis to antitumor effect of paclitaxel. *J Natl Cancer Inst* **88**, 1308–1314.

[19] Chakravarthy A, Nicholson B, Kelley M, Beauchamp D, Johnson D, Frexes-Steed M, Simpson J, Shyr Y, and Pietenpol J (2000). A pilot study of neoadjuvant paclitaxel and radiation with correlative molecular studies in stage II/III breast cancer. *Clin Breast Cancer* **1**, 68–71.

[20] Gore JC, Xu JZ, Colvin DC, Yankeelov TE, Parsons EC, and Does MD (2010). Characterization of tissue structure at varying length scales using temporal diffusion spectroscopy. *NMR Biomed* **23**, 745–756.

[21] Xu J, Does MD, and Gore JC (2009). Quantitative characterization of tissue microstructure with temporal diffusion spectroscopy. *J Magn Reson* **200**, 189–197.

[22] Xu J, Li K, Smith RA, Waterton JC, Zhao P, Chen H, Does MD, Manning HC, and Gore JC (2012). Characterizing tumor response to chemotherapy at various length scales using temporal diffusion spectroscopy. *PLoS One* **7**, e41714. http://dx.doi.org/10.1371/journal.pone.0041714.

[23] Xu J, Does MD, and Gore JC (2009). Sensitivity of MR diffusion measurements to variations in intracellular structure: effects of nuclear size. *Magn Reson Med* **61**, 828–833.

[24] Xu J, Does MD, and Gore JC (2011). Dependence of temporal diffusion spectra on microstructural properties of biological tissues. *Magn Reson Imaging* **29**, 380–390.

[25] Vakifahmetoglu H, Olsson M, and Zhivotovsky B (2008). Death through a tragedy: mitotic catastrophe. *Cell Death Differ* **15**, 1153–1162.

[26] Zhao MZ, Lei CN, Yang YD, Bu XL, Ma HL, Gong H, Liu J, Fang XD, Hu ZY, and Fang QJ (2015). Abraxane, the nanoparticle formulation of paclitaxel can induce drug resistance by up-regulation of P-gp. *PLoS One* **10**.

[27] Schachter M, Does MD, Anderson AW, and Gore JC (2000). Measurements of restricted diffusion using an oscillating gradient spin-echo sequence. *J Magn Reson* **147**, 232–237.

[28] Li H, Gore JC, and Xu JZ (2014). Fast and robust measurement of microstructural dimensions using temporal diffusion spectroscopy. *J Magn Reson* **242**, 4–9.

[29] Beaulieu C and Allen PS (1994). Determinants of anisotropic water diffusion in nerves. *Magn Reson Med* **31**, 394–400.

[30] Hrabe J, Hrabetova S, and Segeth K (2004). A model of effective diffusion and tortuosity in the extracellular space of the brain. *Biophys J* **87**, 1606–1617.

[31] Bocsi J (2009). An introduction to flow cytometry—basic tutorial. *Cytom Part A* **75A**, 719–725.

[32] Allen RT, Hunter WJ, and Agrawal DK (1997). Morphological and biochemical characterization and analysis of apoptosis. *J Pharmacol Toxicol* **37**, 215–228.

[33] Fung AS, Jonkman J, and Tannock IF (2012). Quantitative immunohistochemistry for evaluating the distribution of Ki67 and other biomarkers in tumor sections and use of the method to study repopulation in xenografts after treatment with paclitaxel. *Neoplasia* **14**, 324–334.

[34] Chang J, Ormerod M, Powles TJ, Allred DC, Ashley SE, and Dowsett M (2000). Apoptosis and proliferation as predictors of chemotherapy response in patients with breast carcinoma. *Cancer* **89**, 2145–2152.

[35] Chakravarthy AB, Kelley MC, McLaren B, Truica CI, Billheimer D, Mayer IA, Grau AM, Johnson DH, Simpson JF, and Beauchamp RD, et al (2006). Neoadjuvant concurrent paclitaxel and radiation in stage II/III breast cancer. *Clin Cancer Res* **12**, 1570–1576.

[36] Munk Jensen M, Erichsen KD, Bjorkling F, Madsen J, Jensen PB, Sehested M, Hojgaard L, and Kjaer A (2013). Imaging of treatment response to the combination of carboplatin and paclitaxel in human ovarian cancer xenograft tumors in mice using FDG and FLT PET. *PLoS One* **8**, e85126.

[37] Swanton C, Nicke B, Schuett M, Eklund AC, Ng C, Li Q, Hardcastle T, Lee A, Roy R, and East P, et al (2009). Chromosomal instability determines taxane response. *Proc Natl Acad Sci U S A* **106**, 8671–8676.

[38] Tedeschi PM, Markert EK, Gounder M, Lin H, Dvorzhinski D, Dolfi SC, Chan LL, Qiu J, DiPaola RS, and Hirshfield KM, et al (2013). Contribution of serine, folate and glycine metabolism to the ATP, NADPH and purine requirements of cancer cells. *Cell Death Dis* **4**, e877. http://dx.doi.org/10.1038/cddis.2013.393.

[39] Dolfi SC, Chan LL, Qiu J, Tedeschi PM, Bertino JR, Hirshfield KM, Oltvai ZN, and Vazquez A (2013). The metabolic demands of cancer cells are coupled to their size and protein synthesis rates. *Cancer Metab* **1**, 20. http://dx.doi.org/10.1186/2049-3002-1-20.

[40] Gascoigne KE and Taylor SS (2008). Cancer cells display profound intra- and interline variation following prolonged exposure to antimitotic drugs. *Cancer Cell* **14**, 111–122.

[41] Chenevert TL, Stegman LD, Taylor JMG, Robertson PL, Greenberg HS, Rehemtulla A, and Ross BD (2000). Diffusion magnetic resonance imaging: an early surrogate marker of therapeutic efficacy in brain tumors. *J Natl Cancer Inst* **92**, 2029–2036.

[42] Jiang X, Li H, Xie J, Zhao P, Gore JC, and Xu J (2016). Quantification of cell size using temporal diffusion spectroscopy. *Magn Reson Med* **75**, 1076–1085.

[43] Xu JZ, Li H, Harkins KD, Jiang XY, Xie JP, Kang H, Does MD, and Gore JC (2014). Mapping mean axon diameter and axonal volume fraction by MRI using temporal diffusion spectroscopy. *NeuroImage* **103**, 10–19.

[44] Shaw TJ, Senterman MK, Dawson K, Crane CA, and Vanderhyden BC (2004). Characterization of intraperitoneal, orthotopic, and metastatic xenograft models of human ovarian cancer. *Mol Ther* **10**, 1032–1042.

[45] Lasic S, Nilsson M, Latt J, Stahlberg F, and Topgaard D (2011). Apparent exchange rate mapping with diffusion MRI. *Magn Reson Med* **66**, 356–365.

[46] Lowe SW and Lin AW (2000). Apoptosis in cancer. *Carcinogenesis* **21**, 485–495.

[47] de Bruin EC and Medema JP (2008). Apoptosis and non-apoptotic deaths in cancer development and treatment response. *Cancer Treat Rev* **34**, 737–749.

[48] Portnoy S, Fichtner ND, Dziegielewski C, Stanisz MP, and Stanisz GJ (2014). *In vitro* detection of apoptosis using oscillating and pulsed gradient diffusion magnetic resonance imaging. *NMR Biomed* **27**, 371–380.